

# Automated Cerebellar Lobule Segmentation using Graph Cuts

Zhen Yang<sup>1</sup>, John A. Bogovic<sup>2</sup>, Chuyang Ye<sup>1</sup>, Aaron Carass<sup>1</sup>,  
Sarah Ying<sup>3</sup>, and Jerry L. Prince<sup>1</sup>

<sup>1</sup>Johns Hopkins University, Baltimore, USA

<sup>2</sup>Howard Hughes Medical Institute, Virginia, USA

<sup>3</sup>Johns Hopkins School of Medicine, Baltimore, USA

**Abstract.** The cerebellum is important in coordinating many vital functions including speech, motion, and eye movement. Accurate delineation of sub-regions of the cerebellum, into cerebellar lobules, is needed for studying the region specific decline in function from cerebellar pathology. In this work, we present an automated cerebellar lobule segmentation method using graph cuts, with a region-based term enforcing consistency with multi-atlas labeling results, and a boundary term defined by membership output from a random forest classifier. The region-based term ensures that the location of the lobules conforms to the anatomical convention encoded in the training subjects. The boundary term ensures that the segmentation follows the fine details of lobule boundaries in the subject image. We compared our method to both manual segmentations and a state-of-the-art multi-atlas label fusion technique.

## 1 Introduction

The cerebellum is a piece of the central nervous system that plays an important role in motor control, as well as being involved in flight or fight responses, and for its involvement in cognitive functions [1]. Similar to the cerebrum, the cerebellum function is highly specialized by location. It has also been reported that cerebellar disease and degeneration often target specific regions of the cerebellum and are associated with specific patterns of symptoms [2]. To study these region specific patterns, accurate estimates of the size and shape of the sub-regions of the cerebellum are required, which depends on an efficient delineation of these sub-regions. Like the cerebrum, the cerebellum is divided into two hemispheres with a narrow midline area known as the vermis. The cerebellar cortex consists of a thin sheet of convoluted gray matter (GM) wrapped around white matter (WM) branches emanating from a central mass of white matter called the corpus medullare (CM). Groups of the white matter branches are called lobules which are numbered using roman numerals from I to X, some of which are themselves subdivided such as in the case of Lobule VII. Groups of lobules are referred to as lobes, for example Lobules I through V are the Anterior Lobe, and the boundary between lobes is known as a fissure. Fig. 1 provides an illustration of the cerebellar lobules, as well as magnetic resonance (MR) images of a control

subject and a patient overlaid with cerebellar lobule labels. Note the significant gray matter atrophy in the patient.

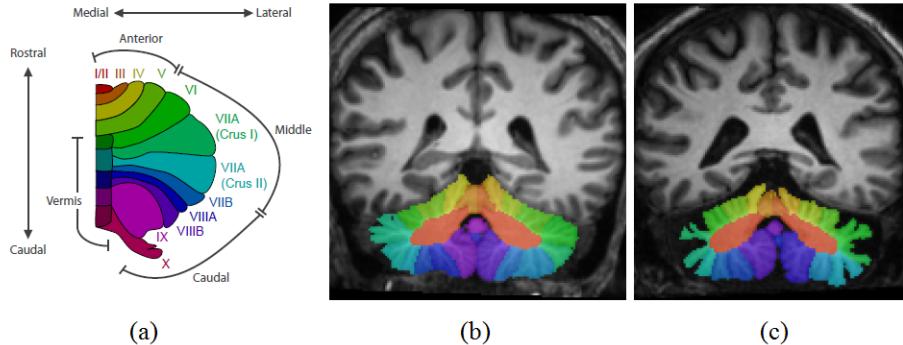


**Fig. 1.** Figures showing (a) an illustration of the cerebellar vermis and lobules (one hemisphere), (b) and (c) MR images of a control subject and a patient overlaid with cerebellar lobule labels.

There has been work on whole cerebellum estimation [3, 4] and identifying cerebellar GM and WM [5]. Although there is great clinical and research utility in labeling the cerebellar lobules, there has been little progress in the automatic segmentation of these regions. Bogovic et al. [6] presented a preliminary demonstration of automatic cerebellum parcellation using a multi-object geometric deformable model but the result was a coarse parcellation of just the lobes and contained no quantitative validation. The state-of-the-art cerebellar lobules segmentation is based on the SUIT atlas of Diedrichsen et al. [7] registered to the subject brain, which may be further improved by using multiple atlases and label fusion techniques [8, 9]. The accuracy of multi-atlas registration based algorithms is limited by the morphological difference between the atlas and subject and the imperfectness of registration. Undesired errors are often made at the boundaries during label fusion because of the lack of constraints on the boundary such as in deformable models [10, 11] and graph cuts [12, 13]. Pierson et al. [14] presented a semi-automated method to segment the cerebellar lobules, though effective it is time consuming which is an undesirable trait.

In this work, we present an automated cerebellar lobule segmentation method using graph cuts, with a region-based term enforcing consistency with multi-atlas labeling results, and a boundary term defined by membership output from a random forest classifier. The region-based term ensures that the location of the lobules conforms to the anatomical convention encoded in the training subjects. The boundary term encourages the segmentation to follow the fine details of the fissures in the subject image. The automated segmentation method produces a 28 label cerebellar parcellation. We validated the algorithm using both control subjects and patients with a cerebellar disease, known as cerebellar ataxia.

Comparison with a multi-atlas label fusion method demonstrates the superior performance of the proposed method.

## 2 Graph Cuts Segmentation

Graph cut methods [12, 13] are widely used in various image segmentation tasks for its robustness and accuracy. It casts the energy-based image segmentation problem in a graph structure and finds the optimal segmentation by efficient min-cut algorithms. In many cases, the energy function includes a region-based term, a boundary term and a label cost term, evaluated for a pixel label assignment  $A$ .  $A$  is a function that maps a pixel  $\mathbf{x}$  to a label  $A(\mathbf{x}) \in \{1, 2, \dots, K\}$ , where  $K$  is the number of labels. The region-based term,  $R(\mathbf{x}, A(\mathbf{x}))$ , evaluates the penalty for assigning label  $A(\mathbf{x})$  to a pixel  $\mathbf{x}$ . The boundary term,  $B(\mathbf{x}, \mathbf{y})$ , evaluates the penalty for assigning a pair of neighboring pixels  $(\mathbf{x}, \mathbf{y})$  with different labels. The energy function can be written as:

$$E(A) = \overbrace{\sum_{\mathbf{x}} R(\mathbf{x}, A(\mathbf{x}))}^{\text{Region-based term}} + \lambda \overbrace{\sum_{\substack{(\mathbf{x}, \mathbf{y}) \in \Gamma \\ A(\mathbf{x}) \neq A(\mathbf{y})}} B(\mathbf{x}, \mathbf{y})}^{\text{Boundary term}}, \quad (1)$$

where  $\Gamma$  is all unordered, neighborhood pixel pairs.  $\lambda \geq 0$  is the weight for relative influence of the two terms.

Fig. 2 shows an example of undirected graph construction from a 2D image. Each pixel in the image is viewed as a node in a graph, edges are formed between neighboring nodes. In addition to the node representing pixels, which we call pixel nodes,  $K$  terminal nodes are constructed to represent the  $K$  labels that to be assigned to the pixels. Edges are also formed between the terminal nodes and all other non-terminal nodes. The energy function for the segmentation problem is encoded in the edge weights of the graph. The region-based term is encoded in the edge weights between terminal nodes and pixel nodes, representing the cost of assigning a label to a pixel. The boundary term is encoded in the edge weights between neighboring pixels, indicating how likely the cut will go between the two pixels. Often the weights between neighboring pixels express how alike two pixels are, given some measure of similarity, as well as the distance between them.

Different cerebellar lobules have very similar intensities, and each consists of inhomogeneous intensities. This makes the lobule segmentation task rather different and more challenging than many graph cuts based segmentation scenarios. Lobules can only be identified by their relative position around the CM and their boundary separated by fissures. To incorporate these observations, in our graph cut formulation, the region-based term  $R(\mathbf{x}, A(\mathbf{x}))$  is derived from a multi-atlas fusion result, which serves as a coarse parcellation of the lobules. The boundary term  $B(\mathbf{x}, \mathbf{y})$  is derived from the boundary membership output by a trained boundary classifier. The final segmentation, which is the min-cut solution to the graph, will then conform to the anatomical convention encoded in the

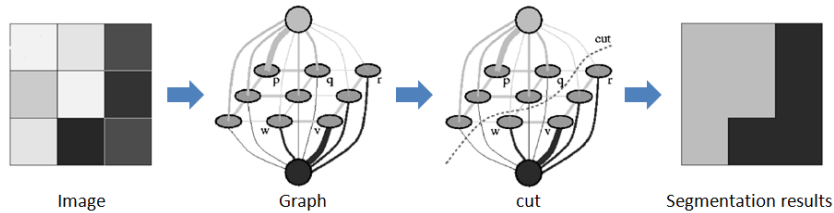


**Fig. 2.** Graph cuts formulation for the segmentation of a  $3 \times 3$  image into two labels. Edge thickness corresponds to the associated edge weight. Images from Boykov et al. [12].

training subjects, and also follow the fine details of lobule boundaries in the subject image. In the next two sections, we will describe in detail the region-based term and the boundary term designed in our graph cut energy function.

### 3 Region-based Term from Multi-atlas Labeling

Multi-atlas based methods have been widely used in segmenting multiple structures in medical images. The idea is to register the images of a set of training subjects to the image of the test subject, and transfer the label of each training subject to the coordinate system of the test subject. Given the transferred labels from the training subjects, segmentation is formulated as a label fusion problem. Voting label fusion strategies, e.g. majority vote, have gained great popularity for its simplicity and robust results. Recently, weighted voting using global, local, semi-local and non-local intensity similarities between the atlases and the target have demonstrated significant improvements in segmentation accuracy [15–17]. Furthermore, statistical fusion strategies have also shown great potential by integrating a model of rater behavior, e.g. the STAPLE algorithm [8] and its many variants [18, 19]. Asman [20] proposed non-local STAPLE (NL-STAPLE), which merges the STAPLE framework with a non-local means perspective and demonstrates significant improvements on segmentation results.

In our work, we use NL-STAPLE to derive the region-based term in graph-cuts. NL-STAPLE models the registered atlases as collections of volumetric patches containing both intensity and label information. It uses the non-local criteria [17, 21] to resolve imperfect correspondence from registration. In the registration process, the intensity image is masked by a smoothed version of the cerebellum mask generated by FreeSurfer. The masked intensity image of each training subject is registered to the test subject, and the label of the training subject is transferred to the coordinate system of the test image. NL-STAPLE is then used to generate a segmentation, represented by  $A_m(\mathbf{x})$ . We design the region-based term in Eq. 1 as follows to penalize label assignment different from  $A_m$ :

$$R(\mathbf{x}, A(\mathbf{x})) = \min_{\mathbf{y}} \|\mathbf{x} - \mathbf{y}\|, \text{ s.t. } A_m(\mathbf{y}) = A(\mathbf{x}). \quad (2)$$

It penalizes a pixel  $\mathbf{x}$  labeled as  $A(\mathbf{x})$  according to its distance to the region labeled  $A(\mathbf{x})$  in the NL-STAPLE segmentation result.

## 4 Boundary Classification

In order to encourage the cuts to be placed along the boundaries of different lobules, it is necessary to distinguish the boundaries of lobules from the rest part of the image, e.g., the inside part of the cerebellum and the background. Ideally an indicator function that equals 1 on the boundaries and 0 otherwise would be desirable. However, it is hard to explicitly model the boundary feature statistics, due to the different boundary appearance between different lobules, and of boundaries between CM and lobules. For example, most of the neighboring lobules are separated by fissures, which can be identified by a low image intensity and high image gradient. However the boundaries between CM and the lobules do not have distinguishable intensity features. In our work, we trained a classifier to detect the boundaries between any pair of structures. The features we used include: 1) image intensity after histogram matching; 2) magnitude of gradient; 3) the trace and determinant of the Hessian matrix; 4) the relative spatial coordinate of the voxel to the centroid of the cerebellar white matter mask estimated by FreeSurfer; 5) signed distance to CM. The CM region in the multi-atlas labeling result is used to compute the signed distance function.

A multi-class random forest [22] classifier is used to classify the image voxels into three classes—boundary, inside cerebellum and outside cerebellum—and estimate the membership of each class. Random forests consist of a set of bootstrap aggregated decision trees and has been shown to achieve robust and accurate classification while avoiding over-fitting. We trained an ensemble of 500 decision trees, with each decision node considering a random subset of 2 of the 8 total input features. The probability that the observation belongs to a particular class can be computed as:

$$q(c|\mathbf{u}(\mathbf{x})) = \frac{1}{T} \sum_{i=1}^T t_i(\mathbf{u}(\mathbf{x}); c), \quad c \in \{\text{b=boundary, i=inside, o=outside}\}, \quad (3)$$

where  $\mathbf{u}(\mathbf{x})$  is the feature vector at voxel  $\mathbf{x}$ . The quantity  $t_i(\mathbf{u}(\mathbf{x}); c) \in [0, 1]$  gives the probability for class  $c$  predicted by the  $i$ th decision tree.

In the training stage, we create a set of training data  $T$  from the training subjects. Each observation in the training data consists of an ordered pair  $(\mathbf{u}(\mathbf{x}), c(\mathbf{x}))$ . For each training subject,  $S$  voxels are sampled for each class, i.e. on the boundary, inside and outside the cerebellum. We chose  $S = 1000$ . Fig. 3 shows the classification result on a test image and the probability of boundary class.

The boundary term in Eq.(1) is designed as

$$B(\mathbf{x}, \mathbf{y}) = 1 - \frac{q(b|\mathbf{u}(\mathbf{x})) + q(b|\mathbf{u}(\mathbf{y}))}{2}, \quad (4)$$

so that the optimal cuts will tend to sever the edge connecting pixels both having high boundary class memberships.

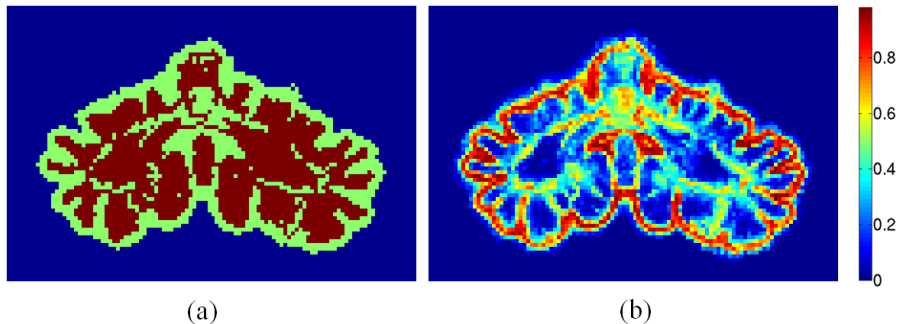


**Fig. 3.** The output of the trained classifier on a test image. (a) Classification result. Green: boundary; red: inside cerebellum; blue: outside cerebellum. (b) Probability of boundary class.

## 5 Graph Cut Optimization

The  $\alpha$ -expansion algorithm [23] has been widely used for multi-label graph cut optimization due to its generality, effectiveness, and speed. The main idea of the  $\alpha$ -expansion is to successively segment all  $\alpha$  and non- $\alpha$ -pixels with graph cuts and the algorithm will change the value of  $\alpha$  at each iteration. The algorithm will iterate through each possible label for  $\alpha$  until the label assignments converges. We use the multi-label energy optimization library available online <http://vision.csd.uwo.ca/code/>. We chose the weight  $\lambda = 2$  in Eq. (1) empirically according the observations in the experiment.

## 6 Results

A cohort of 15 subjects (9 females) is used for training and validation of the proposed algorithm, with ages ranging from 30 to 71 years. Nine of the subjects have been diagnosed with a spinocerebellar ataxia type 6, which is a genetic cerebellar disease. The input images for segmentation are magnetization-prepared rapid gradient echo (MPRAGE) acquired using a 3T MR scanner (Intera, Phillips Medical Systems, Netherlands). The cerebellar lobules of these subjects are manually labeled by a human expert rater, and used as ground-truth for training and validation of the proposed method. Leave-one-out experiments are carried out on the data set, using each subject as test subject and the remaining 14 subjects as training subjects in multi-atlas labeling procedure and to train the classifier for lobule boundaries.

Fig. 4 shows example results of lobule parcellation generated by the algorithm. The segmentations generated by both the NL-STAPLE and the proposed method resemble the manual delineation well. The proposed method shows improvements at lobule boundaries, see the regions in the white box. We also quantitatively evaluate the segmentation results. First we compute the portion

of voxels that are correctly labeled for the whole cerebellum:

$$p = \frac{1}{|M|} \sum_{\mathbf{x} \in M} \delta(A(\mathbf{x}) - A_0(\mathbf{x})).$$

where  $M$  is the set of voxels that labeled non-background in either the automated method or the manual delineation. Table 1 list the portion thus computed for each subject in the leave-one-out experiment for both NL-STAPLE and graph cuts method. The paired Wilcoxon test on the portion numbers produced by NL-STAPLE and Graph cuts shows that Graph cuts improved the segmentation results over the NS-STAPLE results with a p-value of 0.03. The two CB patients, subject 2 and 3, have the lowest portion for correctly labeled voxels. The significant atrophy in cerebellar gray matter affects both the multi-atlas registration and boundary training in an undesirable way. Second, we examine the overlap between the true and automatically obtained labels using the Dice similarity coefficient (DSC). Fig. 5 shows the statistics of the DSC between the manual and automatic labels. We observe that the proposed method improves the NL-STAPLE results in almost all the lobules, especially for the vermis part, e.g. VII vermis, VIII vermis and IX vermis.

**Table 1.** The portion of voxels that are correctly labeled for the whole cerebellum. For the diagnosis, CTRL stands for normal controls, SCA6 for spinocerebellar ataxia type 6, and CB for people who have symptoms of cerebellar dysfunction but no genetic diagnosis or other diagnosis.

Subject No.	1	2	3	4	5	6	7	8
Diagnosis	SCA6	CB	CB	SCA6	CTRL	CB	CTRL	CTRL
NL-STAPLE	0.768	0.607	0.564	0.793	0.733	0.796	0.801	0.785
Graph cuts	0.777	0.614	0.580	0.795	0.739	0.788	0.802	0.786
Subject No.	9	10	11	12	13	14	15	
Diagnosis	SCA6	SCA6	CTRL	Unknown	SCA6	SCA6	CTRL	
NL-STAPLE	0.789	0.689	0.741	0.799	0.695	0.707	0.790	
Graph cuts	0.794	0.745	0.746	0.796	0.693	0.710	0.803	

## 7 Conclusion

We propose an automated cerebellar lobule segmentation method using graph cuts, with a region-based term enforcing consistency with multi-atlas labeling results, and a boundary term defined by membership output from a random forest classifier. The region-based term ensures that the location of the lobules conforms to the anatomical convention encoded in the training subjects. The boundary term ensures that the segmentation follow the fine details of lobule boundaries in the subject image. Comparison with the state-of-the-art multi-atlas labeling method demonstrate the superior performance of the proposed

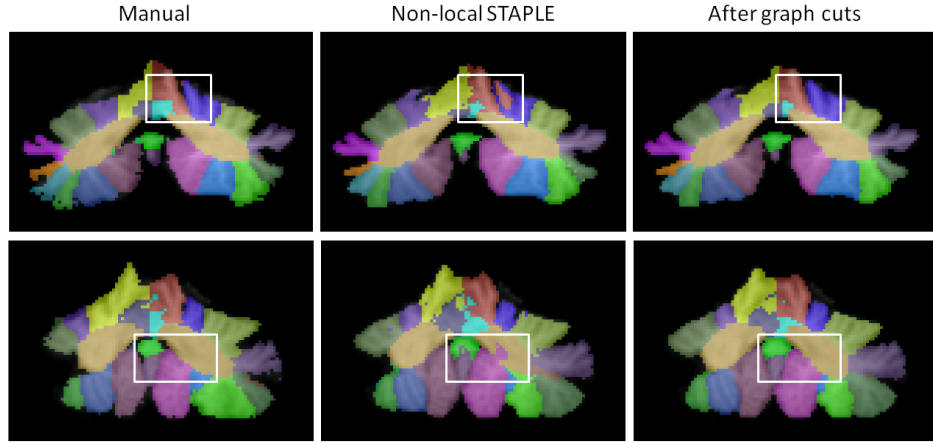


**Fig. 4.** Two coronal slices from two subjects, with lobule segmentation overlaid with intensity image.

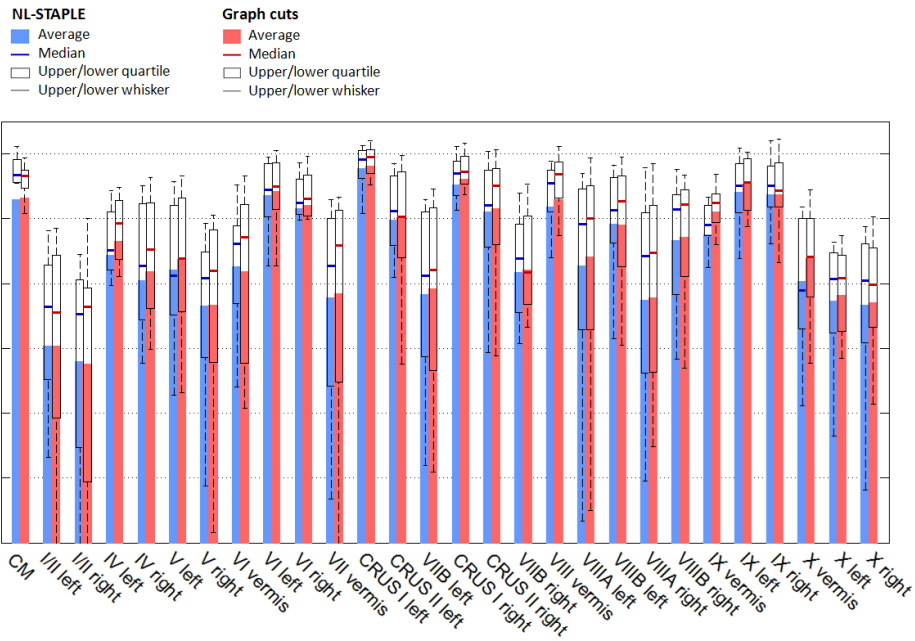


**Fig. 5.** Box plots Dice similarity coefficients.

method. Future work would involve adding atlas selection strategy in the multi-atlas labeling process, so that the subject with significant atrophy can be better registered and segmented.

## 8 Acknowledgment

This work was supported in part by NIH/NINDS grant R01NS056307. We are grateful to Annie Du for her manual delineations of the cerebellar lobules. We also want to thank Andrew Asman and Dr. Bennett Landman for sharing the non-local STAPLE software.

## References

1. Itô, M.: The cerebellum and neural control. Raven Press (New York) (1984)
2. Ying, S., Choi, S., Perlman, S., Baloh, R., Zee, D., Toga, A.: Pontine and cerebellar atrophy correlate with clinical disability in SCA2. *Neurology* **66**(3) (2006) 424–426
3. Ciofolo, C., Barillot, C.: Atlas-based segmentation of 3D cerebral structures with competitive level sets and fuzzy control. *Medical image analysis* **13**(3) (2009) 456
4. Hwang, J., Kim, J., Han, Y., Park, H.: An automatic cerebellum extraction method in T1-weighted brain MR images using an active contour model with a shape prior. *Magnetic Resonance Imaging* **29**(7) (2011) 1014–1022
5. Fischl, B., Salat, D.H., Busa, E., Albert, M., Dieterich, M., Haselgrove, C., van der Kouwe, A., Killiany, R., Kennedy, D., Klaveness, S., et al.: Whole brain segmentation: automated labeling of neuroanatomical structures in the human brain. *Neuron* **33**(3) (2002) 341–355
6. Bogovic, J.A., Prince, J.L., Bazin, P.L.: A multiple object geometric deformable model for image segmentation. *Computer Vision and Image Understanding* **117**(2) (2013) 145–157
7. Diedrichsen, J., Balsters, J.H., Flavell, J., Cussans, E., Ramnani, N.: A probabilistic MR atlas of the human cerebellum. *Neuroimage* **46**(1) (2009) 39–46
8. Warfield, S.K., Zou, K.H., Wells, W.M.: Simultaneous truth and performance level estimation (STAPLE): an algorithm for the validation of image segmentation. *Medical Imaging, IEEE Transactions on* **23**(7) (2004) 903–921
9. Asman, A.J., Landman, B.A.: Non-local STAPLE: An intensity-driven multi-atlas rater model. (2012) 426–434
10. Kass, M., Witkin, A., Terzopoulos, D.: Snakes: Active contour models. *International journal of computer vision* **1**(4) (1988) 321–331
11. Sethian, J.A.: Level set methods and fast marching methods: evolving interfaces in computational geometry, fluid mechanics, computer vision, and materials science. Volume 3. Cambridge university press (1999)
12. Boykov, Y., Funka-Lea, G.: Graph cuts and efficient ND image segmentation. *International Journal of Computer Vision* **70**(2) (2006) 109–131
13. Felzenszwalb, P.F., Huttenlocher, D.P.: Efficient graph-based image segmentation. *International Journal of Computer Vision* **59**(2) (2004) 167–181
14. Pierson, R., Corson, P.W., Sears, L.L., Alicata, D., Magnotta, V., O’Leary, D., Andreasen, N.C.: Manual and semiautomated measurement of cerebellar subregions on MR images. *Neuroimage* **17**(1) (2002) 61–76
15. Artaechevarria, X., Munoz-Barrutia, A., Ortiz-de Solorzano, C.: Combination strategies in multi-atlas image segmentation: Application to brain MR data. *Medical Imaging, IEEE Transactions on* **28**(8) (2009) 1266–1277
16. Isgum, I., Staring, M., Rutten, A., Prokop, M., Viergever, M.A., van Ginneken, B.: Multi-atlas-based segmentation with local decision fusion Application to cardiac and aortic segmentation in CT scans. *Medical Imaging, IEEE Transactions on* **28**(7) (2009) 1000–1010

17. Coupé, P., Manjón, J.V., Fonov, V., Pruessner, J., Robles, M., Collins, D.L.: Patch-based segmentation using expert priors: Application to hippocampus and ventricle segmentation. *NeuroImage* **54**(2) (2011) 940–954
18. Asman, A.J., Landman, B.A.: Robust statistical label fusion through consensus level, labeler accuracy, and truth estimation (COLLATE). *Medical Imaging, IEEE Transactions on* **30**(10) (2011) 1779–1794
19. Landman, B.A., Asman, A.J., Scoggins, A.G., Bogovic, J.A., Xing, F., Prince, J.L.: Robust statistical fusion of image labels. *Medical Imaging, IEEE Transactions on* **31**(2) (2012) 512–522
20. Asman, A.J., Landman, B.A.: Non-local statistical label fusion for multi-atlas segmentation. *Medical image analysis* (2013)
21. Buades, A., Coll, B., Morel, J.M.: A non-local algorithm for image denoising. In: *Computer Vision and Pattern Recognition, 2005. CVPR 2005. IEEE Computer Society Conference on. Volume 2., IEEE* (2005) 60–65
22. Breiman, L.: Random forests. *Machine learning* **45**(1) (2001) 5–32
23. Boykov, Y., Veksler, O., Zabih, R.: Fast approximate energy minimization via graph cuts. *Pattern Analysis and Machine Intelligence, IEEE Transactions on* **23**(11) (2001) 1222–1239